ELSEVIER

Thalamus & Related Systems 1 (2001) 39–52

Thalamus & Related Systems

www.elsevier.com/locate/tharel

Dendritic organization in thalamocortical neurons and state-dependent functions of inhibitory synaptic inputs

M. Neubig*, A. Destexhe

Laboratoire de Neurophysiologie, Faculté de Médecine, Université Laval, Laval, Que., Canada G1K 7P4

Abstract

GABA-ergic thalamic reticular neurons function *generically* or *singularly* in a state-dependent manner: during quiet sleep they synchronously and rhythmically inhibit thalamocortical neurons (TCNs) via bursts, thereby eliciting the low-threshold Ca^{2+} potentials in TCNs that are crucial to oscillatory network behavior in the thalamo-reticulo-cortical system; during wakefulness they shape the flux of ascending sensory information by inhibiting TCNs with asynchronous and arrhythmic single-spikes. To investigate how the reticulo-thalamic synapses, which occur throughout TCN dendrites, are able to effect such disparate functions, we have: (1) used a 1416 compartment model of a 3D reconstructed TCN; (2) triggered dendritic miniature (TTX-independent) and unitary (single-afferent) conductance-based synaptic events, and (3) recorded axial currents and voltage transients in all 1416 compartments simultaneously. For synapses at all dendritic locations, more than 79% of the charge transfer reached the soma, where it dispersed into other dendritic trees to return to the extracellular space. In accord, dendritic synapses in 80% of the arbor induced voltage responses that were severely attenuated at the soma (>75% loss). Spatio-temporal aspects of distributed postsynaptic responses were examined as well. Except for synapses in the 13 most proximal compartments, the amplitude and phase of the voltage responses degraded rapidly within a focal region that did not extend beyond the host tree, and was limited most often to a subtree. The bulk response (outside the focal region) was highly synchronous and uniform. Interestingly, there were not 1403 different focal regions, but only 20, each clearly distinct from the rest and sharply delineated. Structural attributes of the arbor determined their boundaries. Boundaries were invariant when the analysis was repeated on rescaled versions (length, diameter) of the reconstructed arbor. Unitary events also induced focal/bulk structures for both burst and single-spike triggers — paradigms that correspond to single-afferent drives during quiet sleep and arousal, respectively. Such qualities differ dramatically from previously proposed motifs of dendritic clustering, each of which carried nonlinear sensitivities to parameter values. We propose that dendritic clustering underlies the role of reticulo-thalamic synapses in the early processing of ascending sensory information and that bulk responses contribute robustness to the induction and maintenance oscillations in the thalamo-reticulo-cortical network.

Keywords: Sleep; Arousal; Oscillations; Dendritic clusters; Postsynaptic potentials

1. Introduction

Miniature and unitary (single-afferent) inhibitory postsynaptic responses in thalamocortical neurons (TCNs) have been characterized experimentally in several recent reports (Cox et al., 1997; Kao and Coulter, 1997; Kim and McCormick, 1998; Kim et al., 1997; LeFeuvre et al., 1997; Leresche, 1992; Pfrieger et al., 1992; Turner and Salt, 1998; Ulrich and Huguenard, 1996, 1997b; Zhang et al., 1997). Using in vitro current- and voltage-clamp micropipette techniques, these studies have focused on transients at the soma. Here, in addition to somatic transients, we examine the distributed postsynaptic response as it develops throughout a TCNs dendritic arbor in response to inhibitory drives, with the aim understanding how the inhibitory synapses mediate disparate, state-dependent functions.

Individually, TCNs receive 4000–8000 synapses, one-third of which are GABA-ergic and derive from local interneurons and thalamic reticular neurons (TRNs) (Liu et al., 1995; Sato et al., 1997). The proportion attributable to either source varies between species. Of the TRNs, it is thought that each forms ~60 synapses with each of its many target TCNs (Kim and McCormick, 1998; Kim et al., 1997). Based on these numbers, individual TCN receive input from up to 20 to 40 TRNs.

During oscillatory states of the thalamo-reticulo-cortical (TRC) network such as non-REM sleep (Steriade and Deschênes, 1984), TRNs function generically by synchronously and rhythmically hyperpolarizing TCNs. The hyperpolarization is essential to the oscillatory dynamics because the deep potentials enhance de-inactivation of

* Corresponding author. Present address: Computational Neurobiology Laboratory, Salk Institute for Biological Studies, La Jolla, CA 92037, USA. Tel.: +1-858-453-4100/ext. 1124; fax: +1-858-587-0417.
E-mail address: neubig@salk.edu (M. Neubig).

1472-9288/01/$ – see front matter
PII: S1472-9288(01)00005-X

T-type low-voltage activated Ca^{2+} channels (Coulter et al., 1989; Crunelli et al., 1989; Jahnsen and Llinás, 1984). From the de-inactivated state, T-channels are able to mediate rebound low-threshold Ca^{2+} potentials (rLTCPs), which often culminate in a short burst of conventional Na^{+}/K^{+} action potentials (Domich et al., 1986; typically 3–4 spikes). During induction of oscillatory states, few TRNs would be participating, and the inhibitory drive on any given TCN is likely to be spatially non-uniform. The non-uniformity would not be an issue if T-channels were centrally located, such as in the soma. However, recent patch recordings indicate that T-channels are located primarily in the dendrites, with relatively few being located in the soma (Williams and Stuart, 2000). A dendritic localization, which is consistent with earlier in vitro and computational findings (Destexhe et al., 1998; Munsch et al., 1997; Zhou et al., 1997), places a premium on spatially uniform inhibition since it would uniformly prime the T-channels for rLTCP generation.

Interestingly, the same TRNs that trigger rLTCPs during quiet sleep have a different function during wakefulness when TRNs function singularly. In this state TRN inhibition is characterized by asynchronous, arrhythmic, single-spike firing. Studies on the ventrobasal complex in rats, which is a somatosensory structure whose sole source of inhibition is the thalamic reticular nucleus (Harris and Hendrickson, 1987; Ohara and Lieberman, 1993), have shown that TRN driven inhibition contributes to the processing of ascending sensory information (Funke and Eysel, 1998; Hicks et al., 1986; Lee and Ebner, 1992; Lee et al., 1994; Salt, 1989; Worgotter et al., 1998). In this case, local interactions in the dendrites between inhibitory and excitatory synapses are considered to be important.

By approaching the issue of dual-functions (rLTCP generation versus dendritic computations) with computational methods applied to a reconstructed TCN, we have been able to make recordings at hundreds of dendritic locations simultaneously, thereby characterizing the spatial-temporal organization of the postsynaptic response. We used this approach for TTX-independent miniature events and single-afferent unitary events and observed organizational patterns that could be considered counter-intuitive to the generally accepted view that these neurons are electrically compact (we provide results based on recordings of axial currents and somatic transients that resolve these differences). Results are discussed in terms of their significance for thalamic function during sleep and arousal.

2. Methods

Standard computational methods were applied to a model of a 3D reconstructed ventrobasal thalamic relay neuron from a p10 rat (Fig. 1). This particular reconstructed

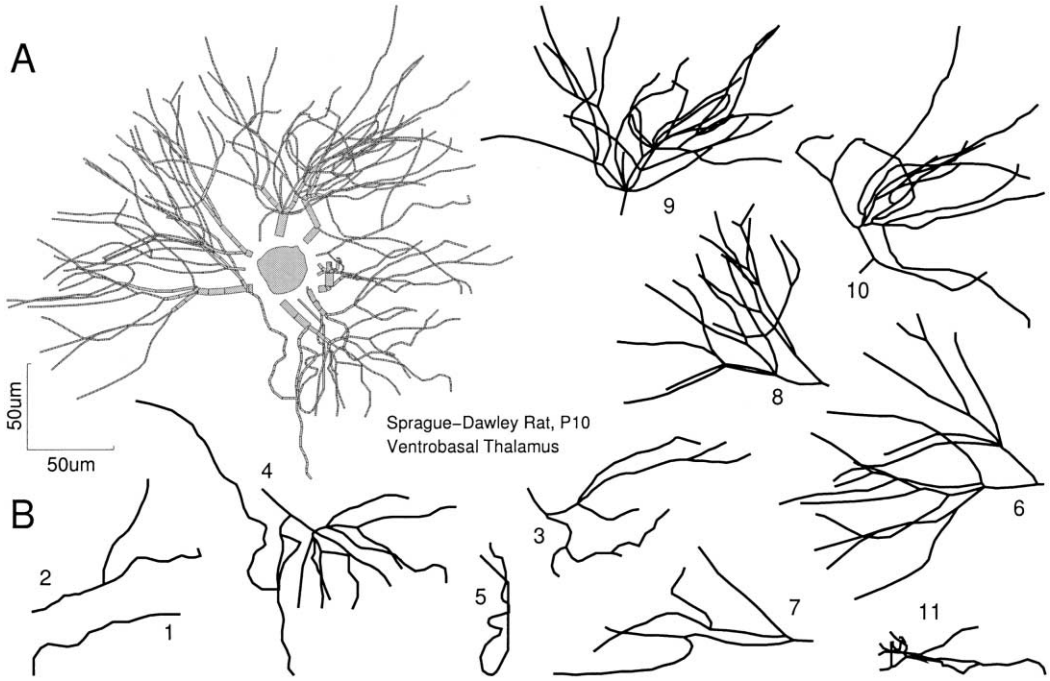

Fig. 1. 3D reconstructed thalamocortical neuron. 3D reconstruction of a thalamocortical neuron (TCN) from the rat ventrobasal complex. Voltage-clamp traces that had been recorded before biocytin filling (Huguenard and Prince, 1992) were used to constrain the passive properties of the model, as detailed in our previous publications. The soma supports a number of dendritic trees, which is stereotypic of TCNs of any nucleus (Jones, 1991; Ohara and Havton, 1994a). Eleven primary dendrites of the reconstructed thalamocortical neuron tended to be either sparsely (1, 2, 3, 5, 7, 11) or profusely (4, 6, 8, 9, 10) branched. (A) Dendrites have been lifted off the soma, the diameter of which is shown reduced by 6% to reflect its net surface area. (B) Individual trees shown unrotated and at same scale as A; numbered in the order in which they were digitized from 80 μm serial sections; to cross-references A and B, use the orientation of its stem as a key.

morphology has been used in our previous studies, where reconstruction details and various electrophysiological aspects may be found (Destexhe et al., 1998; Neubig, 1999a; Neubig and Destexhe, 1997, 1998a,b, 1999). All constraint data had been obtained from ventrobasal TCNs of 1–3-week-old rats. This is an age by which TCNs have the ability to generate essential low-threshold Ca^{2+} bursting (Perez-Velazquez and Carlen, 1996; Pirchio et al., 1997; Warren and Jones, 1997). To reveal the actual lengths of the dendrites in the morphological figures, arbors were flattened (as opposed to projected) onto the viewing plane using an algorithm that preserved both direction and length. Each branch was divided into k compartments of length $l = L/k$; L = anatomical length, k = least integer such that $l/\lambda \leq M$, $\lambda = \sqrt{[1/(g \times R_a)] \times [A/(\pi \times l)] \times c/4}$, A = compartment membrane area; g = membrane conductance density; R_a = axial resistivity; and c = conversion factor. Setting g, R_a, M to 39 μS/C_m^2, 200 Ω cm, 0.01λ established N = 1416 compartments of length (0.094λ ± 0.0008λ), range: 0.01λ–0.0109λ, or 5.00 ± 0.67 μm; range 11.02–1.00 μm. These membrane parameter values were obtained by fitting the model to *recordings from the same neuron* (details in our previous studies, cited above). Soma to dendritic tip paths comprised 19 ± 6 compartments, range 3–36. Considering the number of inhibitory synapses received by TCNs (Liu et al., 1995; Sato et al., 1997) and their uniform areal density (Neubig, 1999b), a resolution of 0.01λ corresponded to one synapse per compartment on average. All trials were run under Linux on a Pentium II box using Neuron (Hines and Carnevale, 1997) with a fixed time-step of 25 μs, except where noted.

Synaptic currents were generated by conductance injections, which are known as *dynamic current clamps* (Sharp et al., 1992, 1993a,b) when implemented in in vitro experiments

$$I_{syn} = I(t, V_m) = g_{syn}(t) \times (V_m - E_{syn})$$

$$g_{syn}(t) = \mathrm{pk}\frac{(e^{-(t+s-on)/(f/q)} - e^{-(t+s-on)/(r/q)})}{fct}$$

Here V_m = perisynaptic membrane voltage, E_{syn} = Cl^- reversal potential, pk = peak conductance amplitude; on = synapse firing time; r, f = time-constants of rise and decay; q = temperature correction of kinetics = $Q_{10}^{(°C-21)/10}$; fct = normalizing factor so that g_{max} = pk; d = 2% down shift of time course s.t. $I_{syn} = 0$ after a finite interval; s = left shift of the time course to compensate for d. Unless indicated otherwise, all membrane and passive properties were uniform.

3. Results

Throughout this study, we use a computational model of a 3D reconstructed thalamocortical neuron (mTCN) (Fig. 1) and emulate dendritic synaptic currents using one or more dynamic current clamps. First, we will present: (i) results on the efficacy with which the dendritic structure of TCNs can disperse charge, as revealed by axial dendritic currents and synapse-to-soma voltage attenuation, and (ii) results which explain the source of some misconceptions about the electronic structure of TCNs. Then we will present a characterization of the distributed postsynaptic response to TTX-independent miniature inhibitory postsynaptic currents, as revealed by simultaneous voltage recordings throughout the neuron (N = 1416 dendritic sites plus one somatic site). Last, we will present results on the distributed postsynaptic response to single-afferent unitary inhibitory postsynaptic currents corresponding to the drive of a thalamic reticular neuron during wakefulness (asynchronous, arrhythmic, single-spike firing) and during quiet sleep (synchronous, rhythmic, burst firing).

3.1. Conductance based synaptic currents

Previously, we had developed a dynamic clamp model of TTX-independent miniature Cl^- currents of *GABA*-ergic reticulo-thalamic synapses in TCNs (Neubig, 1999b) under the constraint of in vitro data (Cox et al., 1997; LeFeuvre et al., 1997; Leresche, 1992; Ulrich and Huguenard, 1996, 1997a). These dynamic clamp currents (I_{syn}), which are sometimes referred to as "conductance injections", were given by the product of a double exponential conductance time course and an Ohmic drive, with peak conductance and time constants of 312 × 10^{-6} pS, 0.1 and 13.9 ms (21°C, Q_{10} = 2.1), respectively (see Section 2). Under a reversed chloride potential, these parameters had yielded a median peak current of 12.1 pA and median 10–90% rise time of 0.98 ms, and time-to-peak of 2.18 ms (Neubig, 1999b). For comparison, the corresponding values obtained in vitro were 12.2 ± 1.3 pA (peak amplitude), 2.0 ± 0.3 ms (time-to-peak), and 13.9 ± 1.4 ms (decay time constant) (Cox et al., 1997; LeFeuvre et al., 1997). In the results presented here, the synapses were triggered from rest and at 36°C, using the reversal potential of $GABA_A$-receptor mediated currents in TCNs, as measured through perforated patches (−81 ± 2.6 mV; cation-selective ionophore gramicidin) (Ulrich and Huguenard, 1997a).

3.2. Dispersion of synaptic charge

We began with a rather simple paradigm. Single events were generated alternately at 1416 dendritic locations, as defined by the arbor's compartmentalization (Fig. 2A). For each event, perisynaptic and somatic voltage transients were recorded, as was the axial current entering/exiting the soma through the stem dendrite of the host tree (Fig. 2C inset).

Site dependency of local input resistance led to site-dependent synaptic currents (identical conductance time courses were used). Grossly, synaptic currents at more distal sites were smaller than those at proximal sites, with peak amplitudes ranging from 6.0 to 6.2 pA (Fig. 2B).

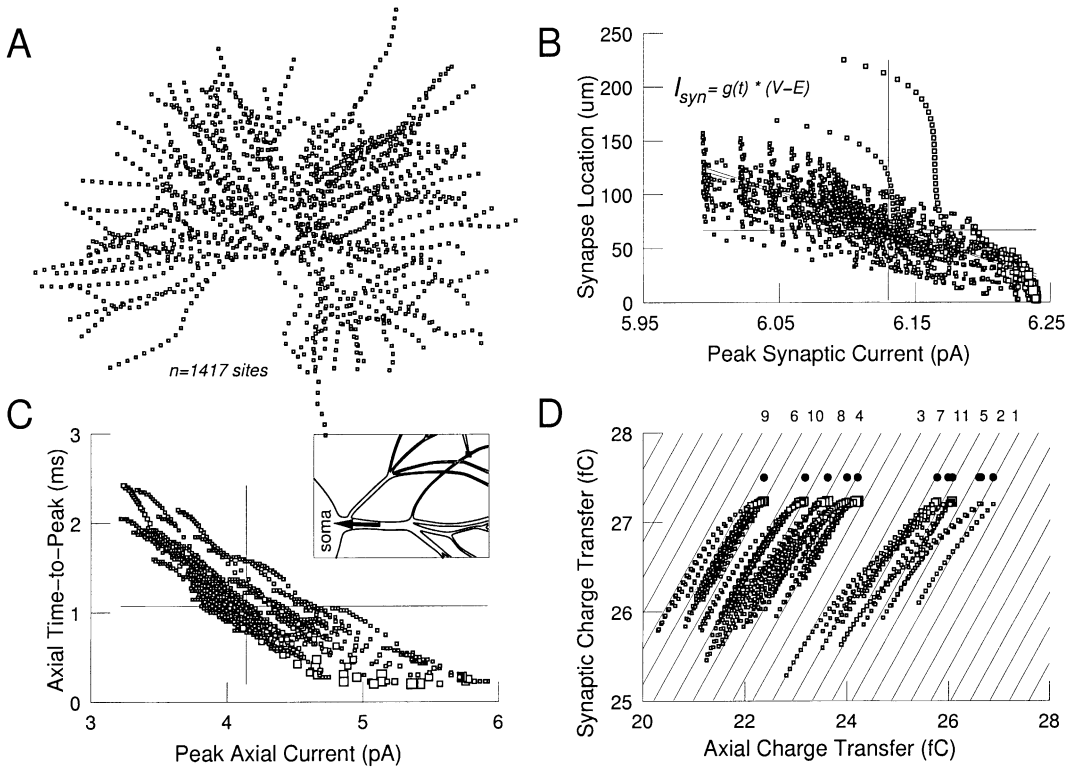

Fig. 2. Efficient dispersion of synaptic charge. TTX-independent miniature synaptic currents were generated in a manner analogous to in vitro dynamic current clamping, by injecting a conductance based current ($I_{syn}(t, V_m)$) that we had developed previously (Neubig, 1999b) under the constraint of in vitro recordings of $GABA_A$ miniature IPSCs (Cox et al., 1997; LeFeuvre et al., 1997; Ulrich and Huguenard, 1996). (A) $I_{syn}(t, V_m)$ was injected at each of 1416 sites alternately; identical conductance time courses were used. (B) Due to local input resistances, peak amplitudes of $I_{syn}(t, V_m)$ were site-dependent. (C) Relationship between amplitude and time-to-peak of the axial current entering the soma (inset). (D) Net charge transfers carried by the synaptic and axial currents. Clustering reflects size differences amongst the dendritic trees; indices correspond to Fig. 1B; *diagonal lines* in the background are drawn with slope of 1 to illuminate the differential organization of profusely vs. sparsely branched trees in terms of charge dispersion, (9, 6, 10, 8, 4; vs. 3, 7, 11, 5, 2, 1). In profusely branched trees, the fraction reaching the soma is equal to the net synaptic flux, minus an offset ($x = y + b$), whereas in sparsely branched trees, the fraction is a percentage of the net synaptic flux, minus an offset ($x = my + b$; $m < 1$). The area of each square is proportional to the compartment's membrane area; due to the constant areal density of inhibitory synapses in TCNs (Neubig, 1999b), these areas are proportional to the number of inhibitory synapses in each compartment. Using this relation, large cross hairs here and throughout indicate weighted medians.

Times-to-peak were 0.15 ms to within half a time step ($dt = 25\,\mu s$).

At its peak, the axial current entering the soma ranged from 3.2 to 5.9 pA (times-to-peak: 0.2–2.4 ms) (Fig. 2C). Given the 6.0–6.2 pA range of event amplitudes, this suggested that more than half of the net synaptic charge flux returns to the extracellular space after passing through the soma and out into the other dendritic trees. To quantify the charge transfers, the axial and the synaptic currents were integrated over their time courses. For the axial current entering the soma, the charge ranged from 20 to 27 fC (mean of 23 fC) (Fig. 2D), which corresponded to 79–99% (mean 86%) of the net synaptic fluxes.

Amongst the eleven trees, differences in total membrane area were reflected in the clustering of data points in Fig. 2D; indices above the graph cross-reference to Fig. 1B. From left to right, the trees comprise 20, 17, 15, 13, 13, 6, 5, 5, 2, 2 and 1% of the arbor's membrane area (21 400 μm). A gap between sparsely and profusely branched trees was apparent. The anatomical difference corresponded to an electrophysiological difference as well: in the graph, most branches on the extensive trees (9, 6, 10, 8, 4) had slopes equal to 1, as revealed by the background lines. On the other hand, most branches in the less extensive trees (3, 7, 11, 5, 2, 1) had slopes less than one.

3.3. Voltage attenuation at the soma

At the synapses, the perisynaptic voltage transients peaked at 0.1–2.1 mV (Fig. 3A). Times-to-peak of the perisynaptic transients ranged widely, from 0.3 to 8.7 ms (Fig. 3B), with most of the variation occurring amongst sites within the proximal dendrites (compare Fig. 3A and B). Regardless of the synapse site, voltage excursions at the soma were uniformly miniscule and slow, with peaks varying between 72 and 83 mV in amplitude and between 8.7 and 10.5 ms in latency (solid black squares in Fig. 3A and B). Although the range of peaks at the soma was narrow in absolute terms (Fig. 3A), they represented a wide variation in attenuation relative to the perisynaptic voltage

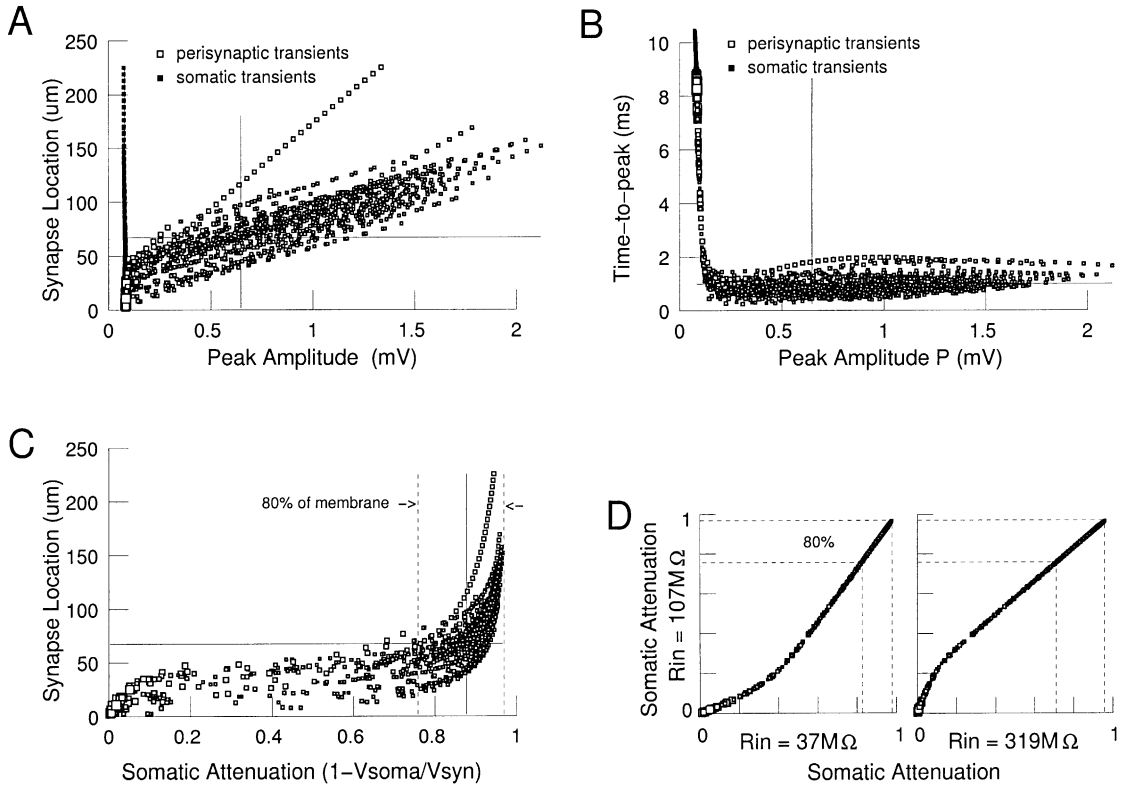

Fig. 3. Severe synapse-to-soma voltage attenuation. Perisynaptic and somatic voltage responses were characterized for TTX-independent miniature synaptic currents by using the paradigm given in Fig. 2. (A) Grossly, peaks of the perisynaptic transients (white squares) are related linearly to remoteness. Somatic transients, which would be analogous to in vitro current clamp recordings, have miniscule peaks (black squares). (B) The wide variation in perisynaptic peaks (white squares) is not reflected in the somatic transients (black squares), neither is the variation in perisynaptic times-to-peak. (C) Relation between synapse location and peak somatic transient relative to the peak perisynaptic transient. Note that 80% of the synapses produce severely attenuated (>75%) voltage signals at the soma. (D) The attribute of severe attenuation is not sensitive to amount of leak current; leak conductance densities of 0.33 and 3 times the baseline (39 $\mu S/C_m^2$) changed the somatic input resistances as indicated, which correspond to TCNs under several experimental paradigms in vivo (30–50 MΩ s), in vitro (100–130 MΩ s) and in vitro with cesium based solutions (300–400 MΩ s). Dashed lines in (C, D) are drawn at the 0th and 80th percentiles.

transient (Fig. 3C). As with the temporal variation mentioned above, most variation in the somatic attenuation occurred amongst synapses within the proximal dendrites. Interestingly, the proximal dendrites are dominated by excitatory synapses carrying ascending sensory systems; in some thalamic nuclei, this is the only region contacted by them (see Section 4).

Reducing or increasing the leak conductance by a factor of three led to nearly identical synaptic currents, and to similar axial current statistics (3.0–5.9 pA at 0.2–2.3 ms and 3.2–5.9 pA at 0.2–2.5 ms) as shown in the somatic attenuation cross-plots (Fig. 3D).

Before going on to the spatio-temporal organization of postsynaptic responses, we note that 80% of the dendritic arbor hosted synapses whose signals at the soma were attenuated by more than 75% relative to the perisynaptic transient (Fig. 3C and D: dashed lines). This is an important statistic because the voltage deflection at the soma will be shown to be representative of the way most of the arbor responds to an individual synaptic event (the exception to this is the membrane area in the focal region near the synapse itself). In this manner, the somatic transient will be a key indicator of the bulk response of the neuron.

3.4. Complete versus partial morphologies

In the only previous modeling study of attenuation in TCNs (Bloomfield and Sherman, 1989), it had been reported that potentials generated anywhere in a TCN dendritic arbor spread with relatively little attenuation throughout the arbor. In that paper, steady-state dc current injections at a given dendritic tip gave rise to variable voltage attenuations elsewhere, with losses averaging 43% at the soma and 48% at other tips. Such numbers conflict with our demonstration of severe and uniform attenuations under a range of membrane conditions (Fig. 3D).

To investigate whether the conflict resulted from differing conditions and/or stimulation paradigms, we reset the biophysical parameters of our mTCN to values used in their study (Fig. $4A_1$ and A_2) and switched to their stimulus (steady dc current injections at a dendritic tip). Two trials were (Fig. $4A_1$ and A_2; injection at boxed 0.00 loca-

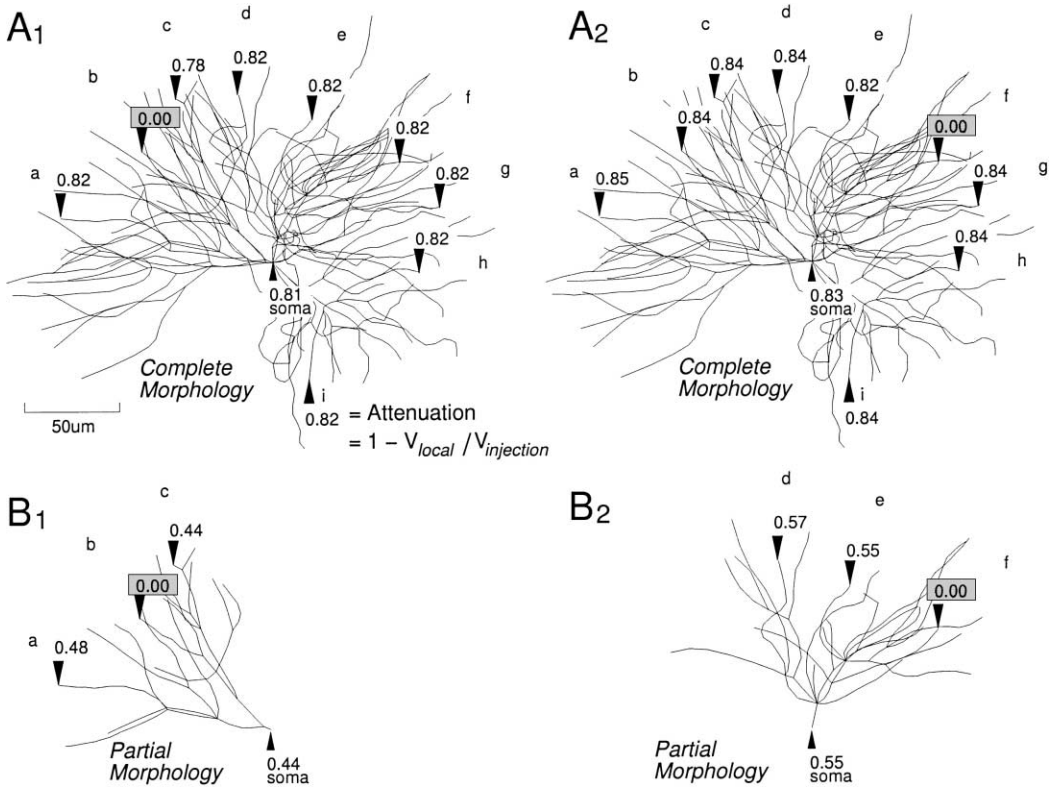

Fig. 4. Steady-state attenuation: complete vs. partial morphologies. The only prior (computational) study on voltage attenuation in TCNs (Bloomfield and Sherman, 1989) had reported mild and variable attenuations (∼45%) throughout TCN dendrites at steady state in response to a dc current injected at a dendritic tip. (A) dc Current injections (boxed locations) produced severe and uniform attenuations during trials on the complete morphology — even when leak conductance density, axial resistivity and specific membrane capacitance were set to the other study's values. (B) Under the hypothesis that their results had been obtained using a model with a soma and a single dendritic tree, partial morphologies were created from the reconstructed arbor. These yielded mild and variable attentions, in accord with their results and suggesting that our hypothesis was correct.

tions) and steady-state voltages were recorded at: (1) tips within the same tree (Fig. 4A_1: (a–c) and A_2: (d–f)); (2) tips within other trees (Fig. 4A_1: (d–i) and A_2: (a–c, g–i)), and (3) the soma. For the complete mTCN, this led to attenuations that were: (i) 1.7 times more severe than their results and, (ii) highly uniform (reflecting, again, the focal and bulk responses).

Because adopting their biophysical parameters and stimuli did not reconcile the differences, we hypothesized that their results were obtained using a partial morphology consisting of a single dendritic tree attached to a soma. To test this, we created two such morphologies by connecting a tree taken from our mTCN to a soma of their dimensions (Fig. 4B_1 and B_2). Using their biophysical parameters, steady dc current injections at a dendritic tip now gave rise to mild and nonuniform steady-state attenuations: 51% on average at tips, and 50% on average at the soma. We conclude that our hypothesis was correct, which underscores the necessity to account for the entire morphology.

3.5. Distributed postsynaptic response

Consequent to a given synaptic event, changes in the membrane voltage take place throughout the entire dendritic arbor. Although these changes commence immediately everywhere, different locations attain different peak levels of hyperpolarization and attain them at different times. In this section, we seek to demonstrate that the spatial distribution of these local peak amplitudes and their timing nearly always divides the arbor into two regions ("nearly always" and "divides" will be put in concrete terms). For reasons that will be obvious, the regions will be termed focal and bulk.

The distributed response for a given synaptic event was assessed by recording 1417 local voltage transients simultaneously: at the synapse, at the soma and at all other dendritic locations as defined by the dendritic compartmentalization (Figs. 1 and 2). For synaptic events at either of the two median sites (Fig. 5A), which are the same as those marked by the cross-hairs in Figs. 2B and 3A, the peaks of the 1417 local transients could be divided into two groups based on either their peak amplitude or on their time-to-peak. Recording sites with attenuation greater than the somatic attenuation spanned 92 and 84% of the membrane, respectively (Fig. 5C). Similarly, slower times-to-peak occurred over 93 and 84% of the membrane (Fig. 5D). The variations of attenuation and timings within these regions were less than 1 and 15% of the overall variation, respectively.

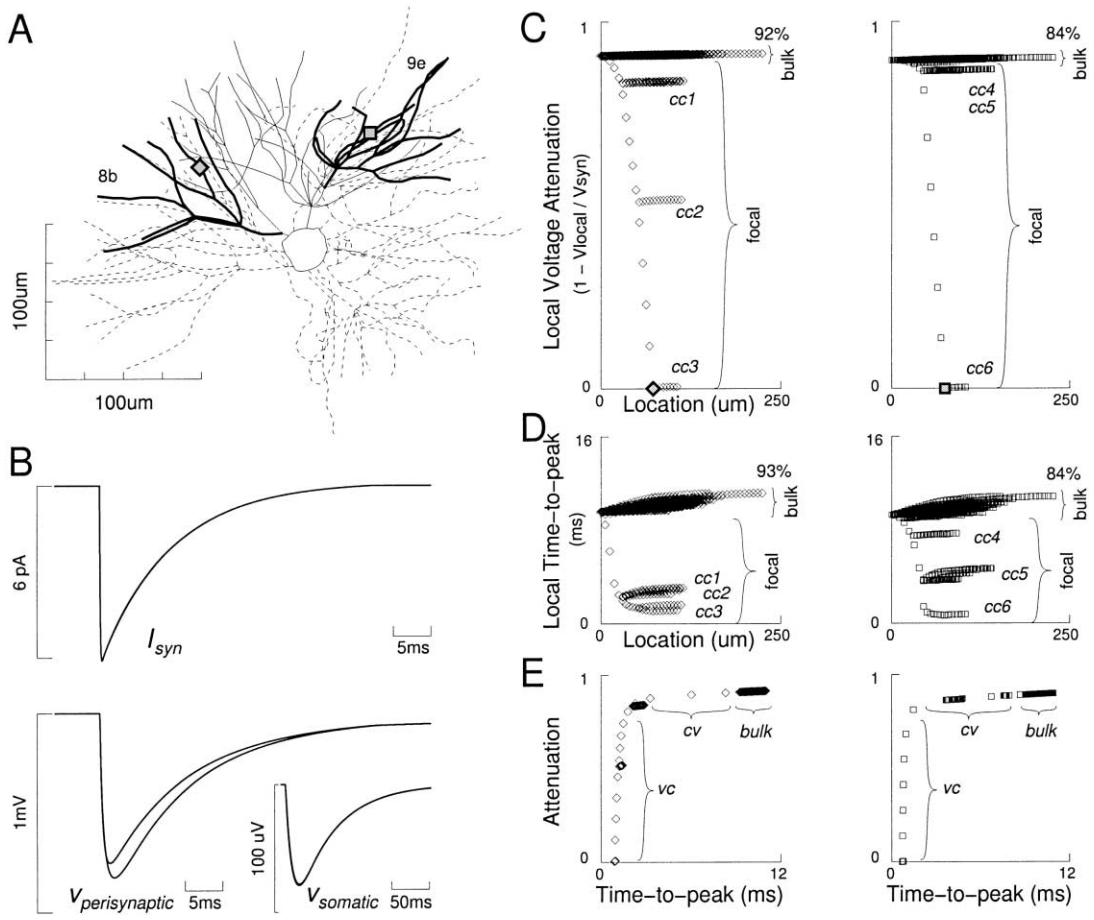

Fig. 5. Scales of structure in the distributed postsynaptic response. For a given synaptic event, the arbor has two qualitatively different regions, designated focal and bulk. The focal region has three qualitatively different subregions, designated cc, cv, and vc, corresponding to regions of constant attenuation, constant phase; constant attenuation, variable phase; and variable attenuation and constant phase, respectively. (A) Location of two synaptic sites for which separate trials were run; the diamond and square are at the sites that were median in Figs. 2B and 3A; *heavy branches* correspond to clustering in Fig. 7; *solid branches* portray the entire tree. (B) Traces, as indicated, from both trials are superimposed in all three plots. (C) Attenuation vs. distance from the soma, based on the 1416 transients that were recorded simultaneously; large diamond and square on the abscissa are data points for the synapse sites themselves; data at cc: 1, 2, 4, 5 are from side branches; data at cc: 3, 6 are distal to the synapse; cut point for focal/bulk domain is the attenuation at the soma (its data point is on the ordinate). (D) Spatial structure of phase of the distributed response is similar to the attenuation structure. (E) The nonlinear, nearly one-to-one relationship between amplitude and phase of the distributed signal reveals two different subregions cv, vc of the focal domain. Note that location of the shoulder in the curve is independent of side branching.

The uniformness of the response over such large extents is the defining characteristic of what will be termed the bulk response. We note here that the domain of the bulk response is not the same for both synaptic events. To show this, the membrane regions that did not constitute the bulk domain — which will be termed the focal domain — are traced as solid lines in the morphology plot (Fig. 5A) (the synapse symbols are embedded in their corresponding focal regions). The focal regions total 1600 and 3500 μm^2, respectively, which equate to 56 and 80% of the membrane of their primary trees. We will show later on that large groups of synapses share, precisely, common focal domains. Here, however, this fact is only suggested by Fig. 5A when one considers the asymmetric extent of the traced lines relative to the synapse position.

In addition to the focal/bulk dichotomy, the focal domain itself has three subdivisions: (1) regions with relatively constant attenuations and constant times-to-peak (Fig. 5C and D: cc1–cc6), (2) regions with varying attenuations but constant times-to-peak (Fig. 5E: vc), and (3) constant attenuations but varying times-to-peak (Fig. 5E: cv). The vc and cv subdivisions demonstrate a way in which the amplitude and temporal qualities can differ in how they structure the dendritic arbor.

The existence of separate bulk and focal responses persists as the synaptic current is generated at sites closer and closer to the soma (Fig. $6A_1$ and A_2). Sibling branches progressively collapse (Fig. 6C) such that for synapses within several tens of microns of the soma (Fig. 6, synapse d), the postsynaptic response partitions the arbor into two regions,

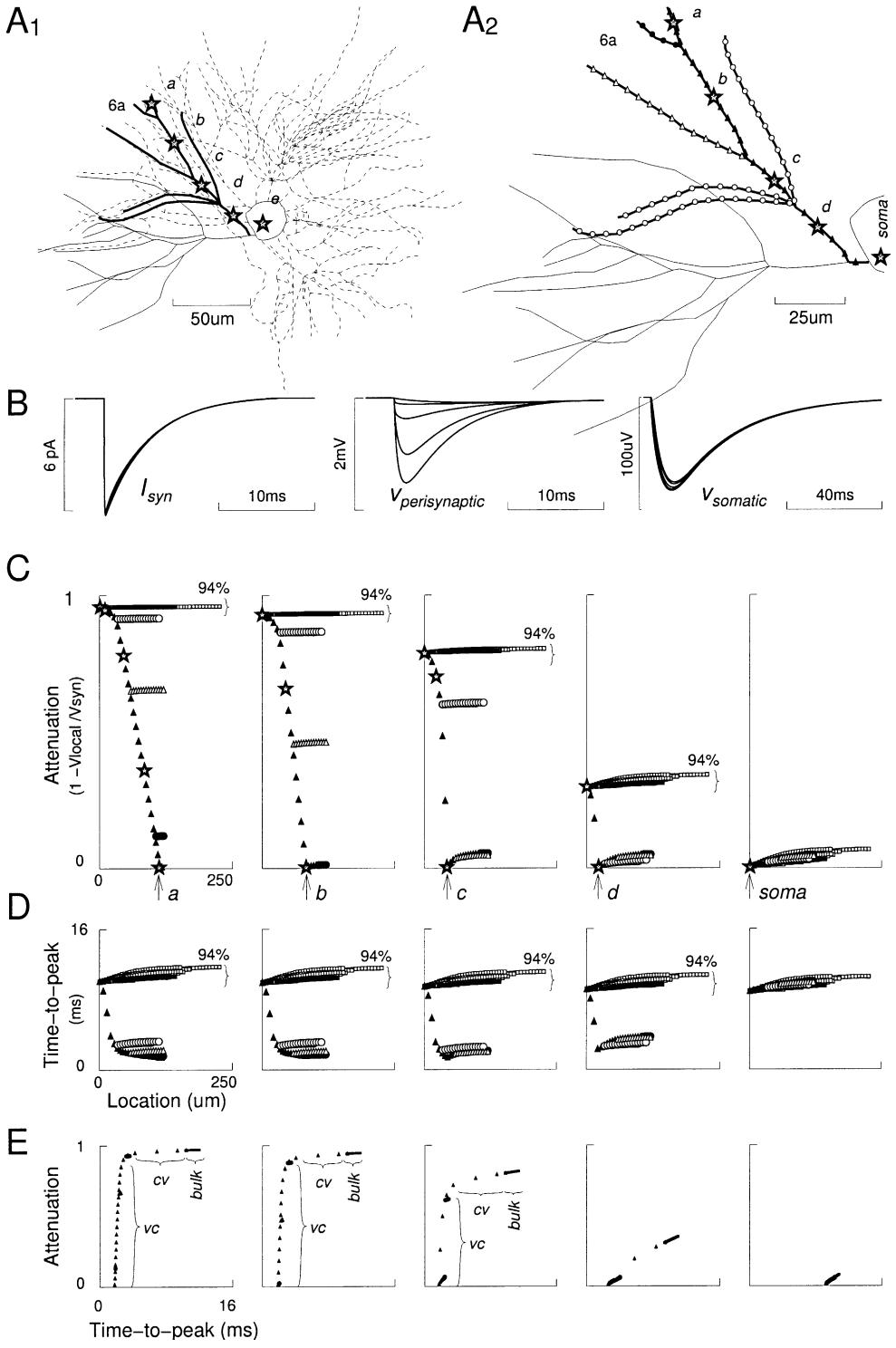

Fig. 6. Spatial robustness of the focal/bulk dichotomy. Broad groups of synapses share common focal and bulk regions, as suggested by this figure and demonstrated later. The five different symbols may be used to cross-reference the panels. The focal and bulk domains remain distinct until the synapse is placed within about 20 μm of the soma. (A_1) Location of five synaptic sites for which trials were run. *Heavy branches* correspond to the clustering in Fig. 7; *solid branches* portray the entire tree. (A_2) The complete host tree drawn at larger scale. (B) Time courses for the five trials are superimposed. (C) Spatial structure of response amplitude. (D) Spatial structure of response phase. (E) Subregions of the focal domain as demonstrated by the amplitude/phase relation, see Fig. 5E.

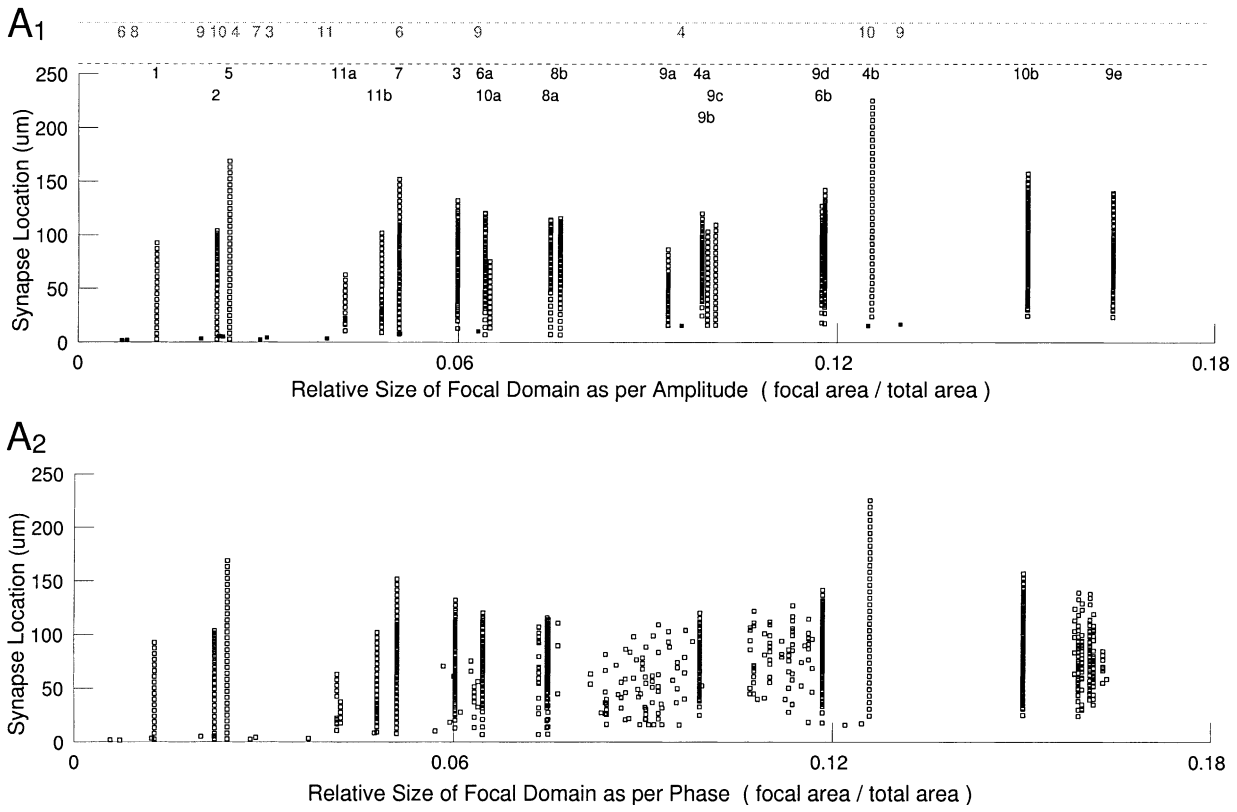

Fig. 7. Dendritic clusters in thalamocortical neurons. Each *square* corresponds to one of the 1416 synapses, and is plotted according to remoteness and focal domain size. (A_1) When defined by response amplitude, 1403 of the synapses (open squares) share one of 20 distinct focal domains, as indicated by the vertical alignments. Dendritic clusters are defined as the membrane area populated by the synapses that share a common focal domain, (not by the membrane area of focal domain itself). For 13 of the synapses (black squares) the focal and bulk domains have coalesced. *Indices* identify the host tree as in Fig. 1; *black indices* pertain to the vertical alignments; grey indices pertain to the scatter at the bottom. (A_2) When defined by response time-to-peak, the clustering structure is similar with 14–16 distinct focal domains, but is less precisely defined in trees 9 and 10, which have large whorls.

each supporting distinct uniform and synchronous responses. The distinction is about an order of magnitude greater than the variability within either region. It is only within the last 10 or 20 μm that the focal and bulk domains coalesce. Within 20 μm of the soma, the net membrane area amounts to 11% of the arbor, which is approximately equal to the somatic membrane area (2400 and 2900 μm^2, respectively).

Irrespective of the synapse's location, the somatic response is always part of the bulk response (Fig. 6C), as alluded to above. Therefore, results from the previous section can be used to understand the overall pattern of the focal/bulk dichotomy. Referring back to Fig. 3C, the most distal synapse capable of inducing a <10% attenuated bulk response is situated at 35 μm. However, the range of bulk responses induced by synapses located within 35 μm of the soma runs as high as 86% in attenuation, which is just below the median bulk response (88%). All synapses situated on 80% of the membrane induce bulk responses characterized by attenuations greater than 75%. The most proximal synaptic location that produces this is at 23 μm, though other synaptic sites at this distance are capable of less than 1% attenuated bulk responses (i.e. a coalesced response).

3.6. Dendritic clusters

Interestingly, the boundaries of the focal domains did not change smoothly as the synapse was moved from one location to the next. In fact, many sites shared identical focal domains, resulting in 20 distinct regions of the arbor. Fig. 7 shows the sizes of focal domains of each synapse as established by amplitude or time-to-peak (Fig. 7A_1 and A_2). The black indices indicate the dendritic tree in which the associated cluster was located. For the present purpose, it is not particularly relevant that the 20 focal domains have different sizes; the key feature is that synapses within a given region of the arbor share a common focal domain. Herein, the term "dendritic cluster" will refer to the aggregate of membrane area populated by a set of synapses which have a common focal domain.

For some synaptic locations near the soma, the focal and bulk domains have coalesced; these appear as the scatter in the bottom of the graphs, and belong to dendritic trees indicated by the grey indices. For the two trees with pronounced whorls (Fig. 1B: 9, 10), focal domains established by the time-to-peak criteria are not in-register, as indicated by the

clouds of scatter in Fig. 7A_2. Next, we created variants of the reconstructed arbor in order to assess the applicability of these results to other TCNs, and to other neuronal types that are characterized in whole or part by bushy architectures (Fig. 8). Diameters were decreased/increased by factors of 0.8 and 1.25 (Fig. 8A_2 and A_3), as were lengths (Fig. 8A_4 and A_5). In each case, the distribution of attenuations as shown in the histograms (severe nearly throughout the arbor), was preserved. Similarly, dendritic clustering persisted under these morphological variations.

3.7. Synaptic drives of single-afferents

In this section, we investigate whether or not the bulk response persists for single-afferent synaptic drives. Unitary inputs were generated by simultaneously triggering 32 synapses identical to those used individually, above. This number was chosen based on the quantity used by Kim et al. ($N = 30$) in their analysis of unitary currents (Kim and McCormick, 1998). Shortly, we will refer to their electrophysiological results for comparative purposes (recall also that the amplitude of each individual synaptic event is based on similar data (Cox et al., 1997)).

The 32 were placed at different locations in the arbor using one of three patterns: (1) clustered: groups of five, randomly in two trees; (2) confined: randomly within one tree; and (3) unconfined: randomly throughout the arbor. To create instances of a pattern, a randomized list of the 1416 dendritic segments was sequentially searched for the first N sites that matched the pattern's criteria. Twenty distinct instances of a each pattern were obtained by beginning the search at staggered (50 entries) starting points; representatives are shown in Fig. 9.

Individual synaptic currents for all three patterns were similar, with the clustered and unconfined patterns having the smallest and largest averages (Fig. 10A, top row). The perisynaptic membranes were more deeply polarized when driven by clustered synapses, and least when driven by the unconfined distribution (second and third rows). However, the opposite trend, albeit diminished, was seen at the soma, where the unconfined distribution was more effective than the clustered distribution.

For all three patterns, single-spike unitary inputs drove the bulk of the membrane through a synchronous and uniform hyperpolarization (fourth row). Moreover, the depth of the bulk hyperpolarization was relatively independent of the pattern of termination (fourth row dashed line). While the bulk response was fairly independent of the synapse pattern (80% circles), the focal response varied between the three as might be expected, with differences primarily in terms of amplitude (outside the 80% circles).

When examined over 20 trials, the somatic transients, which were always part of the bulk response, had mean peak amplitudes of 2.13 ± 0.07, 2.27 ± 0.03 and 2.35 ± 0.01 mV, that occurred at mean times-to-peak of 9.3 ± 0.3, 9.2 ± 0.2, and 9.2 ± 0.2 ms for the clustered, confined and unconfined

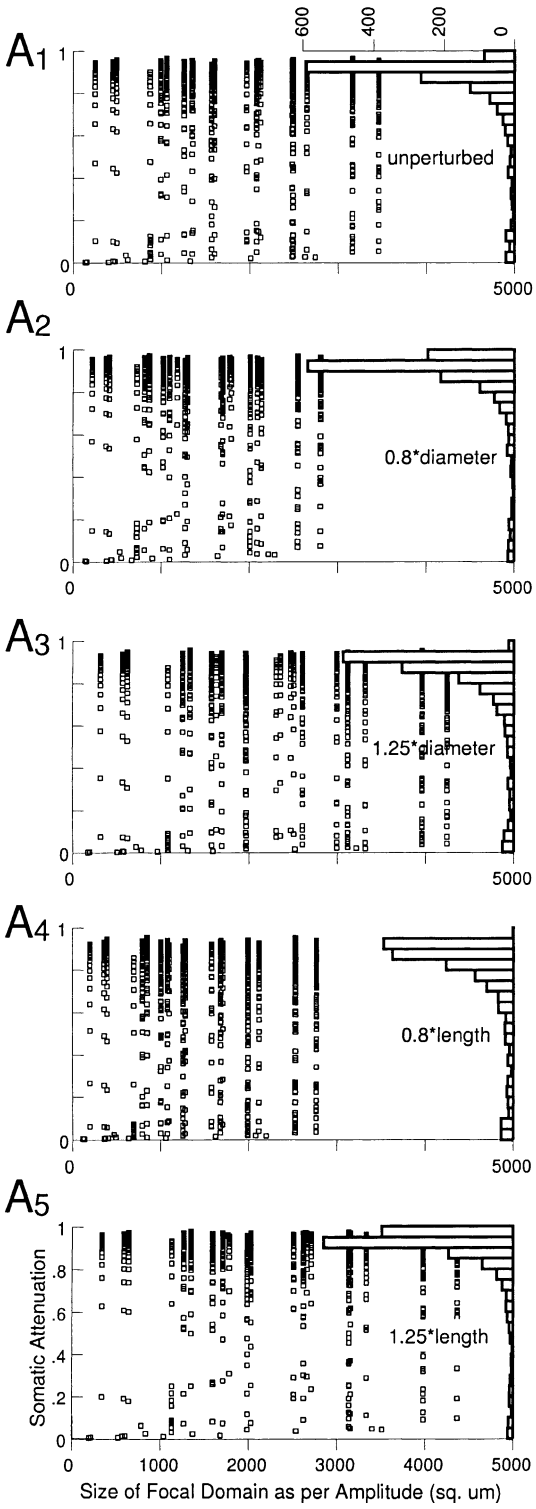

Fig. 8. Invariance of dendritic clusters. To assess the generality of the present results to other thalamocortical neurons, and to other neurons with bushy arbor architectures, the reconstructed arbor (A_1) was used to create four morphological variants (A_2–A_5). The focal/bulk dichotomy persisted in each of the variants, as may be inferred here, where the invariance of dendritic clusters is explicit. The sideways *frequency histograms* of the attenuation of the bulk response demonstrate that each morphological variant is characterized by severe synapse-to-soma attenuation over most of the dendritic arbor.

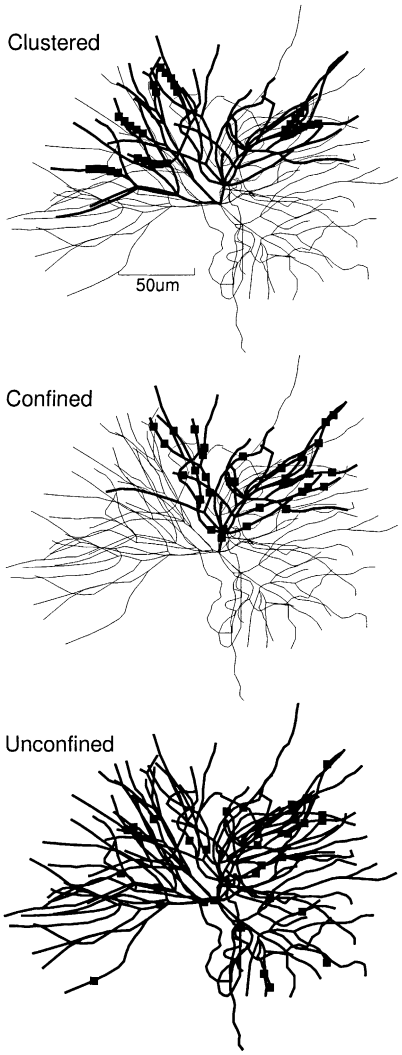

Fig. 9. Termination patterns of synapses from single-afferents. Synapses from a single thalamic reticular axon contact each target TCN at ~60 dendritic locations dispersed along the proximal-distal axis of the arbor and are considered to have a ~50% firing rate (Kim and McCormick, 1998). Termination patterns have not been characterized beyond this. Accordingly, three patterns, each comprising 32 zero-failure rate synapses, were used in examining the distributed response to unitary drives (Fig. 10), namely, *clustered*, *confined*, and *unconfined*. Here, representatives taken from 20 instances of each pattern are shown.

distributions, respectively. These statistics suggest that the variation between different instances of a given pattern is narrower than differences between patterns and that control of the hyperpolarization in the bulk response is dominated by the strength of the drive, not the pattern of termination. For comparison, in vitro unitary responses measured at the soma were approximately 1 mV in amplitude with times-to-peak of 5–10 ms (Kim and McCormick, 1998, similar driving potentials and temperature).

Burst inhibition was examined by repeating single-afferent trials using the same three sets of 20 instances (Fig. 10B). The 32 clamps were triggered six times at 400 Hz, which corresponds to data reported for naturally occurring bursts in thalamic reticular neurons in vitro (350–550 Hz) (Kim and McCormick, 1998). Again, all patterns drove the bulk of the membrane through a synchronous and relatively uniform hyperpolarization. The overall depth of the response was more dependent on the termination pattern than for the single-spike drives. In the present case, the somatic transients, which continued to be part of the bulk response, had mean amplitudes of 7.70 ± 0.41, 8.61 ± 0.19 and 9.27 ± 0.01 mV, that occurred at mean times-to-peak of 17.4 ± 0.6, 17.3 ± 0.5 and 17.4 ± 0.3 ms, for the clustered, confined and unconfined synapse patterns, respectively.

4. Discussion

The first mathematical treatment of dendritic attenuation was carried out in the early 1970s (Rall and Rinzel, 1973; Rinzel and Rall, 1974). Here, we have taken a different approach by applying computational techniques in an experimental (as opposed to mathematical) paradigm. Our present results qualitatively corroborate, build upon and extend beyond the vast body of mathematical analyses whose foundations were established by Wilfred Rall and colleagues (Segev et al., 1995).

TCNs do not meet basic criteria necessary to rigorously reduce reconstructed neurons to simpler forms. In the reconstructed neuron used here, the mean 3/2-power-ratio of dendrite diameters (Rall, 1959) at the 69 branch points was 1.42 ± 0.54, with a range of 0.41–2.84. Under membrane conductances that produce a somatic input resistance of 107 MΩ, the tips of the 108 terminal branches had a mean electronic distance from the soma of $0.17\lambda \pm 0.06\lambda$, with a range of 0.02λ–0.35λ. Other studies on TCNs of other nuclei/species have found similar statistics (Bloomfield et al., 1987; Kniffki et al., 1993; Ohara et al., 1995).

Using an experimental approach, we have started from scratch and characterized the distributed postsynaptic response of a reconstructed thalamocortical relay neuron (Fig. 1) to both miniature (Figs. 2, 3 and 5–8) and unitary (Figs. 9 and 10) inhibitory synaptic drives. We began by recording the axial current entering the soma, demonstrating that even for the most distal synapse, 79% or more of the synaptic current returns to the extracellular space after first passing through the soma and out into the surrounding dendrites (Fig. 2). In accord, voltage attenuations were severe for synapses located anywhere within 80% of the arbor (>75% loss at the soma). Thus, while TCNs are electronically compact (tip-to-soma paths $<0.35\lambda$), "compactness" cannot be interpreted without knowing the neuron's total size (Fig. 4).

The efficient dispersion of charge created a bulk response, characterized by voltage excursions that were highly uniform in both phase and amplitude (Figs. 5, 6, 9 and 10). It also created a focal region surrounding each synapse. Such regions were characterized by a voltage response that rapidly degraded in both amplitude and phase (Figs. 5, 6, 9 and

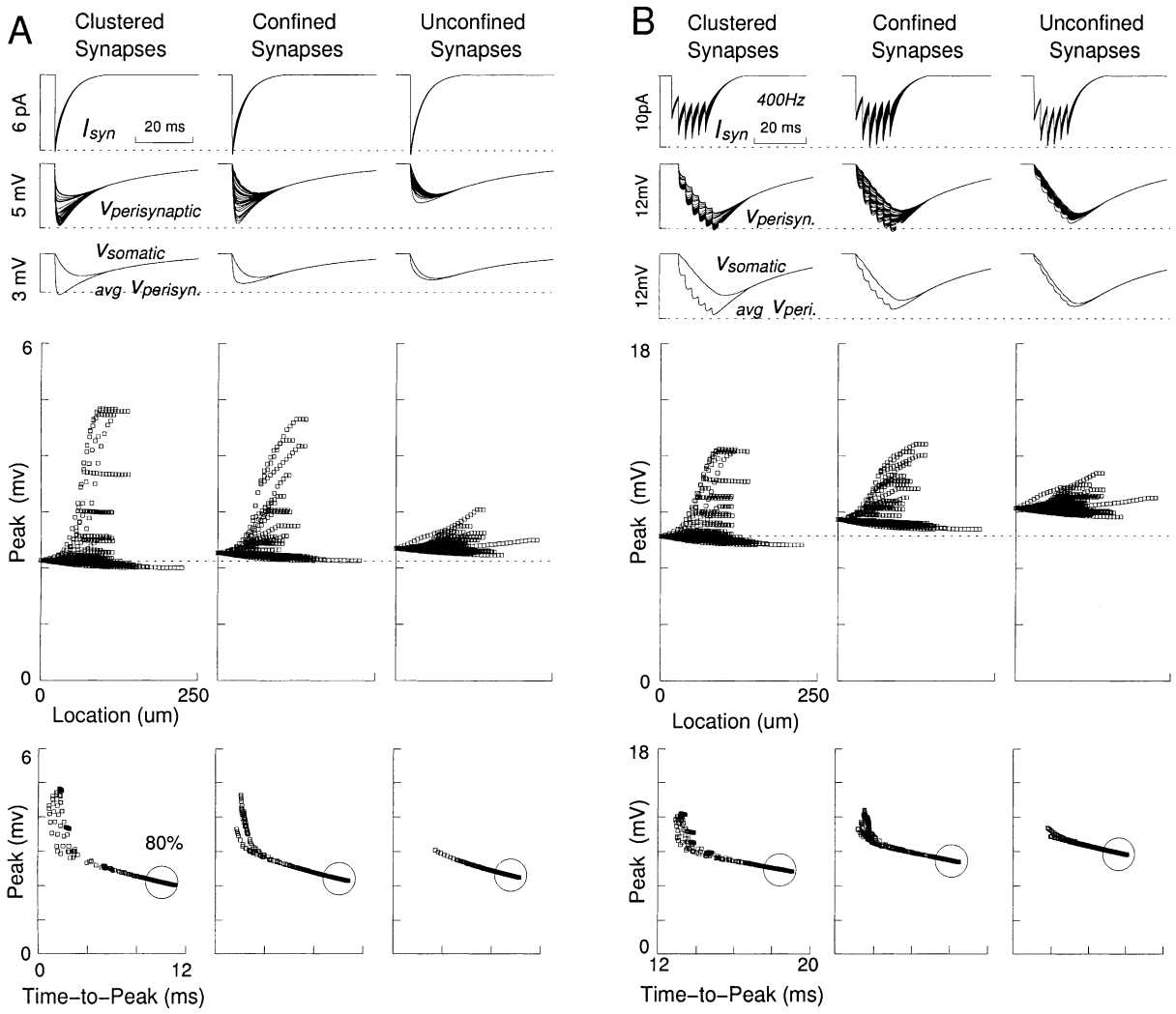

Fig. 10. Amplitude and phase of bulk response is independent of synapse distribution. Multiple synapses (Fig. 9) were triggered simultaneously to generate a unitary response corresponding to input of a single thalamic reticular neuron during wakefulness. The bulk of the membrane reaches approximately the same level of hyperpolarization regardless of the synapse distribution, however the bulk response is distinct from the focal response only when synapses are *clustered*, or *confined*, and not *unconfined*; trials were run on 20 instances of each pattern; selection of synapse locations was otherwise random. (A) Representative trials for single-spike unitary drives that are stereotypical of wakefulness. Superimposed traces of the synaptic currents (top row) and perisynaptic voltage transients (second row), and somatic and average perisynaptic voltages (third row). Note the persistence of the sub-focal structure (Figs. 5 and 6) for the clustered pattern. (fourth row) peak amplitude of the voltage transient in each compartment is plotted as a function of distance from the soma, analogous to Figs. 5D and 6D. (fifth row) Peak amplitude is plotted as a function of time-to-peak, analogous to Figs. 5E and 6E. (B) Representative trials for bursting unitary drives that are stereotypical of quiet sleep. Note again the persistence of the sub-focal structure for the clustered pattern.

10). The focal response occurred primarily along the membrane between the synapse and the soma. The spatially uniform transients that were induced in side branches render each unique by virtue of amplitude and phase (Fig. 5: cc2 and cc3), with exceptions arising anyplace where branching was multifarious (Fig. 5: cc1). Additional structure was seen within the focal domain. The synapse-to-soma path begins with a long region of varying attenuation and constant phase (Figs. 5 and 6: vc) and ends with a short region of constant attenuation and varying phase (Figs. 5 and 6: cv), with the transition point being independent of synapse location (Fig. 6E).

While 1403 of 1416 synapses had well-defined focal domains, each was not distinct; large groups of synapses possessed common focal domains. In fact, there were only 20 distinct domains (Fig. 7) and these were invariant to morphological rescaling (Fig. 8). Synapses sharing a given focal domain defines a dendritic cluster. A lower bound for the number of clusters for any neuron would be the number of trees supported by the soma (11 in the present case). However TCNs comprise a much larger number of dendritic clusters due to their bushy dendritic arbors — *bushy* referring to the short initial and intermediate dendritic branches and the long

terminal branches (TCNs typically have 5–8 orders of branching).

Variants, created by rescaling the morphology, possessed the same clustering structure (Fig. 8). The variants served as controls for any systematic errors or uncertainties in the reconstruction process. Under the relation $\lambda = \sqrt{(R_m/R_a)(\text{diam}/4)}$, the variants also controlled for modulated states of the neuron that are evoked by background levels of synaptic activity and/or by drives from the brainstem and basal forebrain. Though such modulations are not necessarily cell-wide, the robustness of the clustering structure under cell-wide modulations implies robustness under differential modulation of the clusters.

This suggests that dendritic clustering is a feature of TCNs in vivo, when the synaptic drive is more complex than has been considered here, and when active membrane conductances are involved. In this light, each cluster is a separate circuit comprising the inhibitory and excitatory synapses that share a given focal domain (200–400 synapses in the present case) and any active membrane conductances within that region. To a first approximation, each circuit operates independently, with the complexity of the interactions confined within the cluster, and with the net interaction being transmitted out to the soma and the other circuits. The partitioning of the arbor into separate circuits greatly simplifies the constraint of channel densities and individual synaptic weights, and provides for a large repertoire of distinct computations.

There is evidence supporting the existence of a non-trivial repertoire of computations. One would expect: (1) to see several different organizational patterns at the level of dendritic clusters; (2) to see these patterns repeated in different neurons, and (3) to see different groups of these patterns appearing in different subtypes of TCNs. Supporting anatomical evidence includes the distinct branching characteristics amongst different classes of TCNs (Ohara and Havton, 1994a,b) (though all are relatively bushy), and such as the gap between sparsely and profusely branched primary dendrites (as opposed to a continuum) (Fig. 2D) (Havton and Ohara, 1993; Ohara and Havton, 1994a; Ohara et al., 1995).

The division of thalamocortical arbors into robust dendritic clusters does not necessarily obviate the bulk response. Cluster structure seems suited to thalamic function during the awake state, when thalamic reticular neurons are shaping the flux of sensory information in TCNs. During quiet sleep, however, TCNs are drawn into hyperpolarized states by burst inhibition delivered by thalamic reticular neurons. The hyperpolarization enhances the de-inactivation of low-voltage activated Ca^{2+} T-channels, which go on to generate a rebound low-threshold Ca^{2+} spike that finally leads to the output of a short burst of action potentials. The bursts then re-excite the thalamic reticular neurons (though reciprocal connections). These volleys of bursts are essential to oscillatory dynamics of the TRC network.

Since recent patch recordings, optical recordings, and computational results indicate that many T-channels are located in the dendrites (Destexhe et al., 1998; Munsch et al., 1997; Williams and Stuart, 2000; Zhou et al., 1997), the existence of the bulk response ensures that they are uniformly primed (de-inactivated) for low-threshold Ca^{2+} spike generation. The uniformity exists in both the amplitude and phase domains. Further, since the uniformity and amplitude of the bulk response are fairly independent of the location of the synaptic inputs, network oscillations can begin with imprecise participation, and once developed, remain robust against cycle-to-cycle fluctuations in participants. If this description is accurate, then the locations and weights of inhibitory synapses are free to be governed by criteria other than optimization for low-threshold spike activity, such as their role in thalamic function during waking.

Acknowledgements

The authors wish to thank several anonymous reviewers for comments on the manuscript. This work was supported by the Medical Research Council of Canada Grant (MT-13724), National Institutes of Health (RO1-NS37711), and by a research fellowship to MN from Hyrdo-Quebec. Address for reprint requests: M. Neubig, Salk Institute for Biological Studies, CNL, 10010 N Torrey Pines Road, La Jolla, CA 92037, USA.

References

Bloomfield, S.A., Sherman, S.M., 1989. Dendritic current flow in relay cells and interneurons of the cat's lateral geniculate nucleus. Proc. Natl. Acad. Sci. U.S.A. 86, 3911–3914.

Bloomfield, S.A., Hamos, J.E., Sherman, S.M., 1987. Passive cable properties and morphological correlates of neurones in the lateral geniculate nucleus of the cat. J. Physiol. (London) 383, 653–692.

Coulter, D.A., Huguenard, J.R., Prince, D.A., 1989. Calcium currents in rat thalamocortical relay neurones: kinetic properties of the transient, low-threshold current. J. Physiol. (London) 414, 587–604.

Cox, C.L., Huguenard, J.R., Prince, D.A., 1997. Nucleus reticularis neurons mediate diverse inhibitory effects in the thalamus. Proc. Natl. Acad. Sci. U.S.A. 94, 8854–8859.

Crunelli, V., Lightowler, S., Pollard, P.E., 1989. A T-type Ca^{2+} current underlies low-threshold Ca^{2+} potentials in cells of the cat and rat lateral geniculate nucleus. J. Physiol. (London) 413, 543–561.

Destexhe, A., Neubig, M., Ulrich, D., Huguenard, J., 1998. Dendritic low-threshold calcium currents in thalamic relay cells. J. Neurosci. 18 (10), 3574–3588.

Domich, L., Oakson, G., Steriade, M., 1986. Thalamic burst patterns in the naturally sleeping cat: a comparison between cortically projecting and reticularis neurones. J. Physiol. (London) 379, 429–449.

Funke, K., Eysel, U.T., 1998. Inverse correlation of firing patterns of single topographically matched perigeniculate neurons and cat dorsal lateral geniculate relay cells. Vis. Neurosci. 15 (4), 711–729.

Harris, R.M., Hendrickson, A.E., 1987. Local circuit neurons in the rat ventrobasal thalamus — a GABA immunocytochemical study. Neuroscience 21 (1), 229–236.

Havton, L.A., Ohara, P.T., 1993. Quantitative analyses of intracellularly characterized and labeled thalamocortical projection neurons in the ventrobasal complex of primates. J. Comp. Neurol. 336, 135–150.

Hicks, T.P., Metherate, R., Landry, P., Dykes, R.W., 1986. Bicuculline-induced alterations of response properties in functionally identified ventroposterior thalamic neurones. Exp. Brain Res. 63, 248–264.

Hines, M.L., Carnevale, N.T., 1997. The NEURON simulation environment. Neural Comput. 9, 1179–1209.

Huguenard, J.R., Prince, D.A., 1992. A novel T-type current underlies prolonged Ca^{2+} dependent burst firing in GABA-ergic neurons of rat thalamic reticular nucleus. J. Neurosci. 12, 3804–3817.

Jahnsen, H., Llinás, R.R., 1984. Ionic basis for the electroresponsiveness and oscillatory properties of guinea-pig thalamic neurones in vitro. J. Physiol. (London) 349, 227–247.

Jones, E.G., 1991. The anatomy of sensory relay functions in the thalamus. Prog. Brain Res. 87, 29–52.

Kao, C.Q., Coulter, D.A., 1997. Physiology and pharmacology of corticothalamic stimulation-evoked responses in rat somatosensory thalamic neurons in vitro. J. Neurophysiol. 77, 2661–2676.

Kim, U., McCormick, D.A., 1998. The functional influence of burst and tonic firing mode on synaptic interactions in the thalamus. J. Neurosci. 18 (22), 9500–9516.

Kim, U., Sanchez-Vives, M.V., McCormick, D.A., 1997. Functional dynamics of GABA-ergic inhibition in the thalamus. Science 278, 130–134.

Kniffki, K.D., Pawlak, M., Vahle-Hinz, C., 1993. Scaling behavior of the dendritic branches of thalamic neurons. Fractals 1, 171–178.

Lee, S.M., Ebner, F.F., 1992. Induction of high frequency activity in the somatic sensory thalamus of rats in vivo results in long-term potentiation of responses in SI cortex. Exp. Brain Res. 90, 253–261.

Lee, S.M., Friedberg, M.H., Ebner, F.F., 1994. The role of GABA-mediated inhibition in the rat ventral posterior medial thalamus: I. Assessment of receptive field changes following thalamic reticular nucleus lesions. J. Neurophysiol. 71, 1702–1715.

LeFeuvre, Y., Fricker, D., Leresche, N., 1997. $GABA_A$-receptor mediated IPSCs in rat thalamic sensory nuclei: patterns of discharge and tonic modulation by $GABA_B$ autoreceptors. J. Physiol. (London) 502, 91–104.

Leresche, N., 1992. Synaptic currents in thalamocortical neurons of the rat lateral geniculate nucleus. Eur. J. Neurosci. 4, 595–602.

Liu, X.B., Honda, C.N., Jones, E.G., 1995. Distribution of four types of synapse on physiologically identified relay neurons in the ventroposterior thalamic nucleus of the cat. J. Comp. Neurol. 352, 69–91.

Munsch, T., Budde, T., Pape, H.C., 1997. Voltage-activated intracellular calcium transients in thalamic relay cells and interneurons. Neuroreport 8, 2411–2418.

Neubig, M., 1999a. Computational analyses of patterns at the subcellular scale of the electrophysiology of thalamocortical relay neurons. Ph.D. thesis, Faculté de Medecine, Université Laval, Que.

Neubig, M., 1999b. Variation in GABA mini amplitude in thalamocortical neurons: contrasting experimental data and computational analyses. Ph.D. thesis, Faculté de Medecine, Université Laval, Que.

Neubig, M., Destexhe, A., 1997. Constraining morphological and biophysical parameters via minimization along behavioral metrics: low order compartmental models of thalamic relay neurons which preserve afferent synapse distributions. Soc. Neurosci. Abstr. 23, 230–233.

Neubig, M., Destexhe, A., 1998a. Dendritic calcium currents in thalamic relay cells. In: Bower, J.M. (Ed.), Computational Neuroscience Trends in Research. Plenum Press, New York, pp. 233–238.

Neubig, M., Destexhe, A., 1998b. LTS bursting and the subcellular localizations of T-type Ca^{2+} channels in thalamic relay neurons. Soc. Neurosci. Abstr. 24, 407–410.

Neubig, M., Destexhe, A., 1999. Low threshold calcium T-current IV curve geometry is alterable through the distribution of T-channels in thalamic relay neurons. Neurocomputing 26/27, 215–221.

Ohara, P.T., Havton, L.A., 1994a. Dendritic architecture of rat somatosensory thalamocortical projection neurons. J. Comp. Neurol. 341, 159–171.

Ohara, P.T., Havton, L.A., 1994b. Preserved features of thalamocortical projection neuron dendritic architecture in the somatosensory thalamus of the rat, cat and macaque. Brain Res. 648, 259–264.

Ohara, P.T., Lieberman, A.R., 1993. Some aspects of the synaptic circuitry underlying inhibition in the ventrobasal thalamus. J. Neurocytol. 22, 815–825.

Ohara, P.T., Ralston, H.J., Havton, L.A., 1995. Architecture of individual dendrites from intracellularly labeled thalamocortical projection neurons in the ventral posterolateral and ventral posteromedial nuclei of cat. J. Comp. Neurol. 358, 563–572.

Perez-Velazquez, J.L., Carlen, P.L., 1996. Development of firing patterns and electrical properties in neurons of the rat ventrobasal thalamus. Brain Res. Dev. Brain Res. 91 (2), 164–170.

Pfrieger, F.W., Veselovsky, N.S., Gottmann, K., Lux, H.D., 1992. Pharmacological characterization of calcium currents and synaptic transmission between thalamic neurons in vitro. J. Neurosci. 12 (11), 4347–4357.

Pirchio, M., Turner, J.P., Williams, S.R., Asprodini, E., Crunelli, V., 1997. Postnatal development of membrane properties and delta oscillations in thalamocortical neurons of the cat dorsal lateral geniculate neurons. J. Neurosci. 17 (14), 5428–5444.

Rall, W., 1959. Branching dendritic trees and motoneuron membrane resistivity. Expt. Neurol. 1, 461–527.

Rall, W., Rinzel, J., 1973. Branch input resistance and steady attenuation for input to one branch of a dendritic neuron model. Biophys J. 13, 648–688.

Rinzel, J., Rall, W., 1974. Transient response in a dendritic neuron model for current injected at one branch point. Biophys. J. 14, 759–790.

Salt, T.E., 1989. Gamma-aminobutyric acid and afferent inhibition in the cat and rat ventrobasal thalamus. Neuroscience 28, 17–26.

Sato, F., Nakamura, Y., Shinoda, Y., 1997. Serial electron microscopic reconstruction of axon terminals on physiologically identified thalamocortical neurons in the cat ventral lateral nucleus. J. Comp. Neurol. 388, 6133–6631.

Segev, I., Rall, W., Shepherd, G.M. (Eds.), The Theoretical Foundation of Dendritic Function. MIT Press, Cambridge, MA, 1995.

Sharp, A.A., Abbott, L.F., Marder, E.F., 1992. Artificial electrical synapses in oscillatory networks. J. Neurophysiol. l67 (6), 1691–1694.

Sharp, A.A., O'Neil, M.B., Abbott, L.F., Marder, E.F., 1993a. The dynamic clamp: artificial conductances in biological neurons. Trends Neurosci. 16 (10), 389–394.

Sharp, A.A., O'Neil, M.B., Abbott, L.F., Marder, E.F., 1993b. Dynamic clamp: computer-generated conductances in real neurons. J. Neurophysiol. l69 (3), 992–995.

Steriade, M., Deschênes, M., 1984. The thalamus as a neuronal oscillator. Brain Res. Rev. 8, 1–63.

Turner, J.P., Salt, T.E., 1998. Characterization of sensory and corticothalamic excitatory inputs to rat thalamocortical neurons in vitro. J. Physiol. (London) 501 (3), 829–843.

Ulrich, D., Huguenard, J.R., 1996. $GABA_B$-receptor mediated responses in GAB_A-ergic projection neurones of rat nucleus reticularis thalami in vitro. J. Physiol. (London) 493, 845–854.

Ulrich, D., Huguenard, J.R., 1997a. Nucleus-specific chloride homeostasis in rat thalamus. J. Neurosci. 17 (7), 2348–2354.

Ulrich, D., Huguenard, J.R., 1997b. $GABA_A$-receptor mediated rebound burst firing and burst shunting in thalamus. J. Neurophysiol. l78, 1748–1751.

Warren, R.A., Jones, E.G., 1997. Maturation of neuronal form and function in a mouse thalamo-cortical circuit. J. Neurosci. 17 (1), 277–295.

Williams, S.R., Stuart, G.J., 2000. Action potential backpropagation and somato-dendritic distribution of ion channels in thalamocortical neurons. J. Neurosci. 20 (4), 1307–1317.

Worgotter, F., Suder, K., Zhao, Y., Kerscher, N., Eysel, U.T., Funke, K., 1998. State-dependent receptive field restructuring in the visual cortex. Nature 396 (6707), 165–168.

Zhang, S.J., Huguenard, J.R., Prince, D.A., 1997. $GABA_A$-receptor mediated Cl^- currents in rat thalamic reticular and relay neurons. J. Neurophysiol. 78, 2280–2286.

Zhou, Q., Godwin, D.W., O'Malley, D.M., Adams, P.R., 1997. Visualization of calcium influx through channels that shape the burst and tonic firing modes of thalamic relay cells. J. Neurophysiol. 77, 2816–2825.